PHYSICAL REVIEW D **84,** 015007 (2011)

Predictive signatures of supersymmetry: Measuring the dark matter mass and gluino mass with early LHC data

Daniel Feldman,[1] Katherine Freese,[1,2] Pran Nath,[3] Brent D. Nelson,[3] and Gregory Peim[3]

[1]*Michigan Center for Theoretical Physics, University of Michigan, Ann Arbor, Michigan 48109, USA*
[2]*Texas Cosmology Center, University of Texas, Austin, Texas 78712, USA*
[3]*Department of Physics, Northeastern University, Boston, Massachusetts 02115, USA*

(Received 16 February 2011; published 13 July 2011)

We present a focused study of a predictive unified model whose measurable consequences are immediately relevant to early discovery prospects of supersymmetry at the LHC. ATLAS and CMS have released their analysis with 35 pb^{-1} of data and the model class we discuss is consistent with this data. It is shown that with an increase in luminosity, the LSP dark matter mass and the gluino mass can be inferred from simple observables such as kinematic edges in leptonic channels and peak values in effective mass distributions. Specifically, we consider cases in which the neutralino is of low mass and where the relic density consistent with WMAP observations arises via the exchange of Higgs bosons in unified supergravity models. The magnitudes of the gaugino masses are sharply limited to focused regions of the parameter space, and, in particular, the dark matter mass lies in the range ~(50–65) GeV with an upper bound on the gluino mass of 575 GeV, with a typical mass of 450 GeV. We find that all model points in this paradigm are discoverable at the LHC at $\sqrt{s} = 7$ TeV. We determine lower bounds on the entire sparticle spectrum in this model based on existing experimental constraints. In addition, we find the spin-independent cross section for neutralino scattering on nucleons to be generally in the range of $\sigma^{\rm SI}_{\tilde{\chi}^0_1 p} = 10^{-46\pm 1}$ cm^2 with much higher cross sections also possible. Thus, direct detection experiments such as CDMS and XENON already constrain some of the allowed parameter space of the low mass gaugino models and further data will provide important cross-checks of the model assumptions in the near future.

DOI: 10.1103/PhysRevD.84.015007 PACS numbers: 12.60.Jv, 95.35.+d, 14.80.Ly

I. INTRODUCTION

Unified models of supergravity with gravity mediated breaking of supersymmetry [1] extend the standard model of particle physics and are being tested with the Large Hadron Collider experiments at CERN. As a consequence of the breaking of supersymmetry, one obtains soft masses and couplings of the form [1,2]

$$m_{1/2} = M_3(\Lambda_{\rm U}) = M_2(\Lambda_{\rm U}) = M_1(\Lambda_{\rm U}), \tag{1}$$

$$m_0^2 = m^2_{\tilde{Q}}(\Lambda_{\rm U}) = m^2_{\tilde{L}}(\Lambda_{\rm U}) = m^2_{H_{1,2}}(\Lambda_{\rm U}), \tag{2}$$

$$A_0 = A_{\ldots t,b,\tau}(\Lambda_{\rm U}), \tag{3}$$

where at the unification scale, $\Lambda_{\rm U} \sim 2\times 10^{16}$ GeV, there are universal mass terms for the gauginos of $SU(3)$, $SU(2)$, $U(1)$, denoted by $m_{1/2}$, and universal mass squared terms for scalar fields denoted by m_0^2 (where $\tilde{Q}$ ($\tilde{L}$) stands for squarks (sleptons)), and universal cubic (trilinear) couplings A_0 which multiply the Yukawa couplings of matter fields to the Higgs fields. In addition, a (bilinear) soft Higgs mixing term proportional to μ_0 of the form $B_0\mu_0(H_1H_2 + \text{H.c.})$ arises from the superpotential, where $H_2(H_1)$ are the Higgs doublets which give mass to the up quarks (down quarks and charged leptons). The constraints of electroweak symmetry breaking allow the determination of $|\mu|$ (where μ is μ_0 at the electroweak scale) in terms of M_Z and further one makes the replacement of B_0 by the ratio of the Higgs vacuum expectation values $\tan\beta = \langle H_2^0\rangle/\langle H_1^0\rangle$ leaving minimally four parameters and one sign needed as input to define the model [1,2]

$$m_0, m_{1/2}, A_0, \tan\beta, \text{sign}(\mu). \tag{4}$$

Through renormalization group evolution, one computes the predictions for all the masses of the superpartners and their couplings to each other and to the standard model fields.[1]

Models of supergravity address fundamental questions in particle physics, such as the gauge hierarchy problem, the breaking of electroweak symmetry, and the unification of strong and electroweak forces. In addition, such models also provide a compelling dark matter candidate; the lightest supersymmetric particle (LSP). In particular, the neutralino is a linear combination of gauginos and Higgsinos as follows:

$$\tilde{\chi}^0_1 = n_{11}\tilde{B} + n_{12}\tilde{W} + n_{13}\tilde{H}_1 + n_{14}\tilde{H}_2, \tag{5}$$

where $\tilde{B}$ is the bino, $\tilde{W}$ is the wino and $\tilde{H}_{1,2}$ are the Higgsinos. The neutralino can have the right cross section and mass to provide a natural candidate for the observed

[1]For recent reviews see: [3–6].

density of cold dark matter in the Universe. According to the analysis in [7], the latter has the value

$$\Omega_{\rm CDM}h^2 = 0.1120 \pm 0.0056. \tag{6}$$

Here h is the Hubble constant, H_0, in units of 100 km/s/Mpc, and under the assumption that $\Omega_{\rm CDM} = \Omega_{\tilde{\chi}_1^0}$, one has $\Omega_{\tilde{\chi}_1^0} = \rho_{\tilde{\chi}_1^0}/\rho_c$ where the neutralino density $\rho_{\tilde{\chi}_1^0}$ is in units of the critical density $\rho_c = 3H_0^2/(8\pi G) \sim 2 \times 10^{-29}h^2$ g/cm^3. The measurement of the relic density together with a variety of results from collider experiments provide strong constraints on models of new physics.

In this paper, we study a particular region of the unified supersymmetric parameter space which satisfies all the existing experimental and astrophysical bounds and is testable in the very near future. We focus on the region where the neutralino has a mass in the range $\sim$(50–65) GeV. In this mass range, which is above the Z-pole, when $2m_{\tilde{\chi}_1^0} \lesssim m_h$, in those models that are unconstrained by present experimental data, the relic density of neutralinos is largely governed by the presence of the light CP even Higgs-pole (h-pole) [8,9] through annihilations in the early Universe, schematically:

$$\tilde{\chi}_1^0\tilde{\chi}_1^0 \rightarrow h \rightarrow b\bar{b}, \tau\bar{\tau}, c\bar{c}\ldots(2m_{\tilde{\chi}_1^0} \lesssim m_h) \tag{7}$$

arising from the resonance; however, other channels can contribute in general. Additionally, when $2m_{\tilde{\chi}_1^0} \gtrsim m_h$, the relic density can also be achieved via

$$\tilde{\chi}_1^0\tilde{\chi}_1^0 \rightarrow h, H, A \rightarrow f\bar{f} \tag{8}$$

through the s-channel where the heavier Higgses can play the dominant role [8]. Such annihilations can lead to effects on the relic density when the mass of the pseudoscalar m_A is light, of order a few hundred GeV, which corresponds to the case of large $\tan\beta$. Our analysis will find results consistent with a large range of $\tan\beta \sim (3, 60)$ with the possibility of both a heavy and a light pseudoscalar. We will refer to the collective region of the parameter space, with $|m_{\tilde{\chi}_1^0} - m_h/2|_{\max} \lesssim O(5)$ GeV as the "Higgs-pole region".

With universal boundary conditions at the unification scale, the mass range of the neutralino is confined by mass limits on the other particles in the spectrum. In particular, the light chargino has a bound from LEP of $m_{\tilde{\chi}_1^\pm} \geq 103.5$ GeV [10]. It is known that in models with the minimal supersymmetric field content, the light CP-even Higgs mass has an upper bound of roughly $m_h \lesssim 135$ GeV [11]. The Higgs mass is bounded from below by direct searches at LEP [12] and, more recently, at the Tevatron [13]. We will use a conservative lower bound of $m_h \geq 110$ GeV to allow for the theoretical uncertainty in computing the loop corrections to the Higgs mass. We note that a stricter imposition of $m_h > 114$ GeV would narrow the space of models but has little impact on our generic conclusions. Specifically, the low mass gaugino models we study in the Higgs-pole region will correspond to light neutralino dark matter in the range

$$52 \text{ GeV} \leq m_{\tilde{\chi}_1^0} \leq 67 \text{ GeV} \tag{9}$$

that yields the correct relic density and obeys all other experimental constraints subject to the boundary conditions of Eq. (1)–(3).

Here, we will show explicitly with a dedicated study that this class of low mass gaugino models should either be found or ruled out with early LHC data if the expected luminosity of $\sim$few fb^{-1} is reached at $\sqrt{s} = 7$ TeV. In addition, we will discuss current and upcoming dark matter direct detection experiments which also have the possibility of detecting the neutralino LSP in these models.

The reason the models in the Higgs-pole region can be tested soon is that several important mass scales are low enough to be within the discoverable reach of LHC-7. It is known that in minimal supergravity models the following scaling relation amongst the neutralino LSP, the chargino, next to lightest neutralino, and the gluino masses are satisfied [2][2]

$$2m_{\tilde{\chi}_1^0} \simeq m_{\tilde{\chi}_1^\pm} \simeq m_{\tilde{\chi}_2^0} \simeq \frac{1}{4}m_{\tilde{g}}. \tag{10}$$

For a precise determination of the scaling relations above, one must include loop corrections to the gaugino masses [20,21]. Equation (10) typically holds for a very pure bino LSP, whereas the scaling relations receive significant corrections when the LSP eigenstate has a non-negligible Higgsino component. The constraint of Eq. (10), which we will generalize, is an important guide regarding the types of signatures at the LHC for this class of models. In what follows, we will take the scaling assumption to mean that the mass relations of Eq. (10) (or the generalization thereof, which is included in Eq. (13) in what follows) hold to a good approximation.

Remarkably, in the literature there are rather few studies of the impact on LHC physics from this Higgs-pole region with correspondingly low mass gauginos; only recently has it seen some attention. Thus, some aspects of the minimal supergravity models where the relics annihilate near the light CP-even Higgs-pole have been discussed in Refs. [14–19], which fall under the mass hierarchy denoted by mSP4 (supergravity mass pattern 4) [14,15], where, in particular, a clean edge in the dilepton invariant mass in this model class was noted in Ref. [15]. In addition, the very recent work of Ref. [19] studies electroweak symmetry breaking in an overlapping class of models with a focus on the μ parameter and radiative breaking.

Some of our observations and emphasis here have overlap with Ref. [17] and some are rather different. In

[2]This relation holds for the case when $\mu^2 \gg M_Z^2, M_1^2, M_2^2$ all taken at the electroweak scale.

Ref. [17], emphasis was given to explaining the CDMS-II results and predictions for the XENON data, and in doing so, a slice of the parameter space was studied where $\tan\beta = 50$ and A_0 was fixed for a few choice values, while the analysis allowed for flavor violation, and thus constraints from $b \to s\gamma$ and $B_s \to \mu^+\mu^-$ were not imposed. Our present analysis imposes these constraints and opens up new parameter space where all direct and indirect constraints are satisfied, and where the spin-independent scattering cross section can lead to event rates that can be observed in the XENON detector.

When all direct search limits and indirect constraints on the parameter space are imposed, a number of robust mass relations are predicted. The main points emphasized in this work are as follows:

(1) Two key observables which are directly measurable at the LHC: the peak in the effective mass distribution as well as the dilepton invariant mass edge are shown to be strongly correlated in these models. A first determination of the gluino mass can be measured from the peak value of the effective mass distribution and the dark matter mass can simultaneously be inferred from the dilepton edge due to the predicted scaling relations in the gaugino sector given in Eq. (10).

(2) The recent CMS and ATLAS data with 35 pb^{-1} of integrated luminosity [26,27] do not yet provide constraints on the models discussed in this paper. In the Higgs-pole region, even though the gluino has a low mass, the 2nd generation squark masses are larger than 1 TeV and typically of order several TeV which is the main reason these models remain unconstrained by the CMS and ATLAS data (the gluino mass bounds in the recent ATLAS analysis [27] do not apply to our models). However, we will show that with increased luminosity they will begin to probe such models.

(3) The gluino has a low mass which is tightly constrained to lie in the range $400\ \mathrm{GeV} \lesssim m_{\tilde{g}} \lesssim 575\ \mathrm{GeV}$, with most points having[3] $m_{\tilde{g}} \simeq 450 \pm 20$ GeV. The mass splitting between the gluino and the lighter gauginos is appreciable. Thus, should this model class be realized in nature, the production of jets from the gluino should be seen at the LHC at $\sqrt{s} = 7$ TeV with about a few inverse femtobarns of data [16,22–25], [19].

(4) The chargino mass is bounded from below by the LEP search limits and from above by theory, $m_{\tilde{\chi}_1^\pm} \lesssim 130$ GeV, with the second heaviest neutralino being effectively degenerate with the lightest chargino. This suggests that the associated production of $\tilde{\chi}_1^\pm \tilde{\chi}_2^0$ is sizeable and may reveal itself in multilepton channels, in particular, the trilepton ($3L$) channel [28,29]. The large SUSY breaking scalar masses in the models imply that the current bounds from the Tevatron do not yet constrain the models.

(5) There is a sizable region of the parameter space in which $\tan\beta$ can be large and the pseudoscalar Higgs boson is relatively light. Such model points may allow for simultaneous reconstruction of $m_{\tilde{g}}$ and m_A in early LHC data collection.

(6) The constraints from the CDMS and XENON data [30,31] on the spin-independent scattering cross section of neutralinos on nucleons is complimentary to searches for the CP-odd Higgs at the Tevatron and at the LHC. In fact, for some models in the parameter space the XENON data already constrains models that will be tested in 2011 and 2012 at the LHC. We find many candidate models that yield large event rates in upcoming dark matter direct detection experiments.

As an aside, we note that the neutralino annihilation rate we consider is too low to produce observable cosmic signatures of positrons, antiprotons, or gamma rays; hence recent experimental bounds from a variety of cosmic ray experiments are not a concern. In principle, one could boost the annihilation cross section in a number of ways in order to reach the sensitivity of the experiments, but that approach is not considered here.

We add here that in general there does exist a large collection of possible models and, in particular, a large collection of possible sparticle mass hierarchies [14,15,18]. These of course can give rise to different and interesting signatures, and several previous works have made progress on discussing how such models may be discriminated against one another [14–16,18,49].

In the work presented here, we give a focused study of a dense, i.e. well-populated, region of the parameter space of minimal supergravity models where the LSPs have low mass that also have low mass gluinos which will be tested at the LHC in the very near future. Namely, we will focus on the signatures of models that annihilate via the Higgs-pole that have a relatively light gluino and heavy squarks. Therefore, we show explicit methods for detection of this model. If such experimental observations do not see these explicit signatures, the model can be ruled out. In addition, we find a bound on the Higgs sector from the XENON data. We explore the connection between these models and what the LHC, the Tevatron, and the dark matter scattering experiments can observe. The prominent signatures of the models under full collider simulation are discussed in detail in what follows.

II. ANALYSIS OF THE PARAMETER SPACE AND SPARTICLE MASSES

In this section, we describe our targeted parameter scan over the minimal supergravity parameter space for the low

[3]This is the Gaussian peak (i.e. mean) and Gaussian width (i.e. 1 standard deviation).

mass gaugino models that lie in the Higgs-pole region. We will illustrate the various constraints we have imposed on the models, from astrophysical relic density as well as accelerator bounds. From the results of our survey of parameter space, we then obtain the viable range for sparticle masses and the relations between them.

In the analysis that follows we compute the thermal relic density as implemented in MICROMEGAS 2.4 [32]. We demand that the resulting value of the cold dark matter relic density $\Omega_{\rm CDM}h^2 = \Omega_{\tilde{\chi}_1^0}h^2$ satisfy

$$0.08 \leq \Omega_{\tilde{\chi}_1^0}h^2 \leq 0.14. \tag{11}$$

The spread in (11) around the WMAP band [7] is chosen to allow theoretical uncertainties and sensitivity to the top pole mass, both of which enter in the sparticle spectrum under renormalization group flow and radiative electroweak symmetry breaking.

Our targeted parameter scan over the minimal supergravity parameter space is described in what follows. For models in which the gaugino masses are given by a universal parameter $m_{1/2}$ at the scale $\Lambda_{\rm GUT} \simeq 2 \times 10^{16}$ GeV, the analysis of Refs. [2,33] found that Eq. (10) is consistent with $m_{\tilde{\chi}_1^\pm} \sim m_{\tilde{\chi}_2^0} \sim (0.9 \pm 0.1)m_{1/2}$; thus in the interest of obtaining models with low mass gauginos, we restrict $m_{1/2}$ to the range 100 GeV $\leq m_{1/2} \leq$ 175 GeV. The universal scalar mass was allowed to vary in the range 0.1 TeV $\leq m_0 \leq$ 10 TeV with the upper bound representing a naturalness requirement on the models. The entire allowed range of $\tan\beta$ was explored and the universal trilinear parameter A_0 was allowed to vary over the range $-4 \leq A_0/m_0 \leq 4$. Throughout, we take $\mu > 0$ and $m_{\rm top}^{\rm pole} = 173.1$ GeV. Renormalization group evolution and calculation of the physical masses of the sparticles was performed using SUSPECT [34] and SUSY-HIT [35] was used in the computation of branching ratios of the superpartners.

Our survey resulted in 12 000 parameter sets, each defining a single model. All model points were required to satisfy the requirements of radiative electroweak symmetry breaking. Accelerator constraints were applied as well. The most important bounds include the imposition of the Higgs mass bound discussed in the previous section, and the bound on the chargino mass from direct searches for sparticles $m_{\tilde{\chi}_1^\pm} \gtrsim 103.5$ GeV from LEP [10]. In addition, a number of indirect experimental constraints were imposed, which include those from the Tevatron, Belle/*BABAR*/Cleo and Brookhaven experiments. Specifically we impose the conservative constraints $(-11.4 \times 10^{-10}) \leq \delta(g_\mu - 2) \leq (9.4 \times 10^{-9})$, see [36,37], ${\rm Br}(B_s \to \mu^+\mu^-) \leq 4.7 \times 10^{-8}$ (90% C.L.) [38], and $2.77 \leq {\rm Br}(b \to s\gamma) \times 10^4 \leq 4.27$ [39]. The indirect constraints were calculated using MICROMEGAS, with the standard model contribution in the last observable corrected according to the work of Misiak *et al.* [37,40]. Finally, we require that the relic density satisfy Eq. (11).

The models surveyed are consistent with

$$|m_{\tilde{\chi}_1^0} - m_h/2|_{\max} \leq 7 \text{ GeV}, \tag{12}$$

with most models satisfying $|m_{\tilde{\chi}_1^0} - m_h/2| \lesssim 4$ GeV. Therefore, *post facto*, Eq. (11) and Eq. (12) together provide an effective definition of what constitutes the Higgs-pole region. From this ensemble of models, we find the mass relations

$$\begin{aligned} m_h &= \alpha_h m_{\tilde{\chi}_1^0}, & 1.78 &\leq \alpha_h \leq 2.25 \\ m_{\tilde{\chi}_1^\pm} &= \alpha_{\tilde{\chi}_1^\pm} m_{\tilde{\chi}_1^0}, & 1.65 &\leq \alpha_{\tilde{\chi}_1^\pm} \leq 2.07 \\ m_{\tilde{\chi}_2^0} &= \alpha_{\tilde{\chi}_2^0} m_{\tilde{\chi}_1^0}, & 1.70 &\leq \alpha_{\tilde{\chi}_2^0} \leq 2.07 \\ m_{\tilde{g}} &= \alpha_{\tilde{g}} m_{\tilde{\chi}_1^0}, & 7.34 &\leq \alpha_{\tilde{g}} \leq 9.25 \end{aligned} \tag{13}$$

and the qualitative scaling relations in Eq. (10) can be replaced by the more quantitative relations

$$\begin{aligned} &m_h = \alpha_{\tilde{\chi}_1^0} m_{\tilde{\chi}_1^0} = \beta_{\tilde{\chi}_1^\pm} m_{\tilde{\chi}_1^\pm} (\simeq \beta_{\tilde{\chi}_2^0} m_{\tilde{\chi}_2^0}) = \beta_{\tilde{g}} m_{\tilde{g}} \\ &0.92 \leq \beta_{\tilde{\chi}_1^\pm} \leq 1.17, \qquad 0.22 \leq \beta_{\tilde{g}} \leq 0.29. \end{aligned} \tag{14}$$

The distribution of gluino masses for the models is well approximated by a Gaussian with a remarkably small width. In Fig. 1, we plot the distribution in the dimensionless ratio $\alpha_{\tilde{g}} = m_{\tilde{g}}/m_{\tilde{\chi}_1^0}$ from Eq. (13). We see that, in general, the models produce a gluino mass of

$$m_{\tilde{g}} = (451 \pm 19.5) \text{ GeV}(1\sigma). \tag{15}$$

Thus, consistent with Eq. (10), one finds

$$m_{\tilde{g}}/m_{\tilde{\chi}_1^0} = 7.86 \pm 0.209(1\sigma). \tag{16}$$

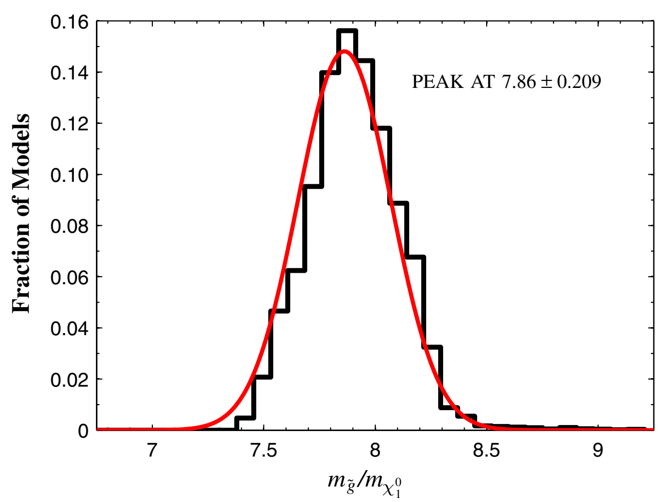

FIG. 1 (color online). Distribution of the ratio $\alpha_{\tilde{g}} = m_{\tilde{g}}/m_{\tilde{\chi}_1^0}$ from Eq. (13). The distribution is well approximated by a Gaussian characterized by $\alpha_{\tilde{g}} = 7.86 \pm 0.209$. The corresponding spread of gluino masses for the models simulated was found to be $m_{\tilde{g}} = (451 \pm 19.5)$ GeV (quoted are mean values and one standard deviation about the mean).

TABLE I. General predictions for the sparticle masses for the models with $m_0 \leq 10$ TeV satisfying all phenomenological constraints discussed in the text. It is further found that $m_0 \geq 1.05$ TeV, and the scalar masses are bounded as: $m_{\tilde{t}_1} \geq$ 323 GeV, $m_{\tilde{b}_1} \geq 706$ GeV, $m_{\tilde{\tau}_1} \geq 484$ GeV, $m_{\tilde{q}} \geq 1070$ GeV, $m_{\tilde{\ell}} \geq 1050$ GeV, and $m_A \geq 187$ GeV.

Mass Predictions (GeV)	Eigencontent of the LSP	
$110 \leq m_h \leq 126$	$0.888 \leq n_{11} \leq 0.996$	$(\tilde{B})$
$52 \leq m_{\tilde{\chi}_1^0} \leq 67$	$-0.163 \leq n_{12} \leq -0.016$	$(\tilde{W})$
$104 \leq m_{\tilde{\chi}_1^\pm} \leq 131$	$0.019 \leq n_{13} \leq 0.396$	$(\tilde{H}_1)$
$396 \leq m_{\tilde{g}} \leq 575$	$-0.167 \leq n_{14} \leq -0.006$	$(\tilde{H}_2)$

In Table I, we expand on the general ranges given in Eq. (13). For example, whereas in the previous paragraph and in Fig. 1 the 1σ error bars are quoted for the gluino mass, the full range of all gluino masses obtained in our survey is

$$396 \text{ GeV} \leq m_{\tilde{g}} \leq 575 \text{ GeV}. \tag{17}$$

The upper bound for the gluino mass, consistent with a low mass neutralino, has very important consequences for LHC searches as discussed in the next section. Another result of our analysis is that while the LSP is dominantly binolike, it can also have a significant Higgsino component as seen from Table I.

For the small values of $m_{1/2}$ that lead to a light gaugino sector, it is necessary to require large m_0 and/or $\tan\beta$ to satisfy the direct search limits on the light CP-even Higgs mass h. We therefore found that $\tan\beta$ ranges from about 3 to 60 and that typically m_0 is much larger than $m_{1/2}$. Indeed, in our survey an empirical lower bound of $m_0 \geq$ 1.05 TeV was obtained. A large fraction of the models thus lie on the hyperbolic branch/focus point region [41] in which scalars are in the TeV range and μ is typically small. Consequently, all the first and the second generation squarks and sleptons are significantly heavier than the gluino. In particular, one finds the lower bounds $m_{\tilde{q}} \geq$ 1070 GeV and $m_{\tilde{\ell}} \geq 1050$ GeV on squarks and sleptons of the first two generations. Third generation squarks and sleptons are also found to be generally heavy, though lower masses occasionally arise for certain combinations of A_0/m_0 and $\tan\beta$. Specifically, we find the following lower bounds on third generation scalars: $m_{\tilde{t}_1} \geq 323$ GeV, $m_{\tilde{b}_1} \geq 706$ GeV and $m_{\tilde{\tau}_1} \geq 483$ GeV.

We further note that the μ parameter for most of the models lies in the range $300 \text{ GeV} \lesssim \mu \lesssim 700$ GeV, though larger values are possible. The models with low μ can lead to a CP-odd Higgs mass m_A that can be quite light—particularly when the value of $\tan\beta$ is simultaneously large. We find a lower limit of $m_A \geq 187$ GeV over the ensemble of models studied. As we will see below, inclusion of the limits on the neutralino-proton spin-independent cross section, $\sigma^{\rm SI}_{\tilde{\chi}_1^0 p}$, from the CDMS and XENON experiments further constrain the models. We discuss this in some detail in Sec. IV.

Finally, one might ask if charginos with masses in the range 104 GeV $\leq m_{\tilde{\chi}_1^\pm} \leq 131$ GeV are already ruled out by direct searches at the Tevatron, given the recently quoted lower bounds of $m_{\tilde{\chi}_1^\pm} \gtrsim 150$ GeV derived from the absence of trilepton events with large missing transverse energy [42–44]. Such a lower bound is due to the assumption of light slepton masses. However, as discussed above, the low mass gaugino models in the Higgs-pole region single out scenarios in which the sleptons are generally very heavy, as in the "large m_0" models analyzed by D0 [43]. Using PROSPINO2 [45] to calculate the next-to-leading order production cross sections for the Tevatron at $\sqrt{s} = 1.96$ TeV we find, before cuts and efficiency factors,

$$1.33 \times 10^{-2} \text{ pb} \leq \sigma(p\bar{p} \to \tilde{\chi}_2^0 \tilde{\chi}_1^\pm)_{\rm NL0} {\rm Br}(\tilde{\chi}_1^\pm \to l^\pm \nu \tilde{\chi}_1^0) \, {\rm Br}(\tilde{\chi}_2^0 \to l^+ l^- \tilde{\chi}_1^0) \leq 5.98 \times 10^{-2} \text{ pb} \tag{18}$$

after simply summing over all three generations of leptonic decay products, which is the maximal case, and this result is below the reported limits from the Tevatron [42–44].

III. SIGNATURES OF THE LOW MASS GAUGINO MODELS IN THE HIGGS-POLE REGION AT THE LHC

To study the signatures of the low mass gaugino models at LHC-7, we simulate events at $\sqrt{s} = 7$ TeV for a sample of 700 model points from the larger set discussed in the previous section. The standard model (SM) backgrounds considered were those used in [24,25] which were done by using a MLM matching with a k_T clustering algorithm. The SM background was generated with MADGRAPH 4.4 [46] for parton level processes, PYTHIA 6.4 [47] for hadronization and PGS-4 [48] for detector simulation. The SM backgrounds compare well to those given in [23]. The total R parity-odd SUSY production cross section ($\sigma_{\rm total}$) for the low mass gaugino models are composed, to a first approximation, of only three contributions: production of chargino and the second lightest neutralino (i.e. $\sigma_{\tilde{\chi}_1^\pm \tilde{\chi}_2^0}/\sigma_{\rm total}$; 47% $\pm$ 2.5%); gluino pair production (i.e. $\sigma_{\tilde{g}\tilde{g}}/\sigma_{\rm total}$; 28% $\pm$ 3.3%); and chargino pair production (i.e. $\sigma_{\tilde{\chi}_1^\pm \tilde{\chi}_1^\mp}/\sigma_{\rm total}$; 23% $\pm$ 1.3%). The three sparticles produced with the largest production modes, namely $\tilde{g}$, $\tilde{\chi}_1^\pm$, and $\tilde{\chi}_2^0$, then decay with the dominant branching ratios shown in Table II. The ranges shown are for the subset of 700 models. The total SUSY production cross section is relatively large for this class of models given the relatively light gluino, charginos and neutralinos ($\sigma_{\rm total}$ = 9.65pb $\pm$ 1.43pb) over the set of 700 models.

The rather small variances around the central values for production cross sections and branching fractions suggest that the models in the Higgs-pole region are strikingly

TABLE II. Typical size of dominant branching ratios of the sparticles with the largest production modes emerging from proton-proton collision at the LHC over a subset of 700 models. Here u, d includes the first 2 generations of quarks and l includes all 3 generations of leptons (hence the factors of 2 and 3 in the Table). The factor of 4 includes u, d and the conjugate modes for the charginos. In addition to the three dominant sparticles produced arising from proton-proton collisions (the three cases considered in the Table), a small subset of models are found to produce light stops ($m_{\tilde{t}_1} \sim 350$ GeV) at the LHC which decay via $\tilde{t}_1 \to (t\tilde{\chi}_1^0, b\tilde{\chi}_1^+, t\tilde{\chi}_2^0)$ respectively, depending on the particular model point.

$\mathrm{Br}(\tilde{g} \to X)$	%	$\mathrm{Br}(\tilde{\chi}_2^0 \to X)$	%	$\mathrm{Br}(\tilde{\chi}_1^\pm \to X)$	%
$u_i\bar{u}_i\tilde{\chi}_2^0$	$2 \times (5.1 \pm 0.38)$	$u_i\bar{u}_i\tilde{\chi}_1^0$	$2 \times (12.5 \pm 0.57)$	$u_i\bar{d}_i\tilde{\chi}_1^0$	$2 \times (33.5 \pm 0.12)$
$d_i\bar{d}_i\tilde{\chi}_2^0$	$2 \times (5.0 \pm 0.3)$	$d_i\bar{d}_i\tilde{\chi}_1^0$	$2 \times (16.3 \pm 0.88)$	$l\nu_l\tilde{\chi}_1^0$	$3 \times (11.0 \pm 0.07)$
$b\bar{b}\tilde{\chi}_2^0$	15.1 ± 2.47	$b\bar{b}\tilde{\chi}_1^0$	16.1 ± 1.88		
$u_i\bar{d}_i\chi_1^- + \mathrm{H.c.}$	$4 \times (10.1 \pm 0.75)$	$l^+l^-\tilde{\chi}_1^0$	$3 \times (2.9 \pm 0.49)$		
$t\bar{b}\tilde{\chi}_1^- + \mathrm{H.c.}$	$2 \times (5.5 \pm 1.2)$	$\nu_1\bar{\nu}_l\tilde{\chi}_1^0$	$3 \times (5.7 \pm 1.09)$		

TABLE III. Four benchmarks to illustrate collider and dark matter signals of the low mass gaugino models in the Higgs-pole region. All models give a suitable relic density consistent with WMAP. Masses and dimensionful input parameters are given in units of GeV. The first and second generation squarks are denoted by $\tilde{q}$. The top pole mass is set to 173.1 GeV and the sign of μ is positive. Number in the table are rounded to the nearest integer. All values are computed with MICROMEGAS 2.4 and SUSPECT.

Label	m_0	$m_{1/2}$	A_0	$\tan\beta$	$m_{\tilde{g}}$	m_h	$m_{\tilde{\chi}_1^0}$	$m_{\tilde{\chi}_1^\pm}$	$m_{\tilde{q}}$	$m_{\tilde{t}_1}$	$m_A \simeq m_H$
1	2990	148	2503	26	476	119	60	117	2959	1668	2608
2	1238	132	−2007	7	407	116	55	109	1250	421	1467
3	2463	133	−2003	50	447	118	58	117	2443	1353	423
4	2839	131	−2401	50	451	119	58	118	2812	1562	355

similar in their features, at least in terms of the phenomenology associated with the gaugino sector. This is not unexpected given previous studies of sparticle mass hierarchical patterns [14,15,18,49]. As we will demonstrate in what follows, these similarities allow predictions to be made if excesses over SM background are observed at the LHC. Furthermore, as we will see in Sec. IV, it is likely that these models will allow for a determination of the light gaugino masses and a partial determination of the neutralino LSP's eigencontent should a corroborating signal be observed in dark matter direct detection experiments.

To illustrate the phenomenology of the low mass gaugino models in the Higgs-pole region, it is important to look at several signature channels to corroborate evidence for discovery. As such, we have chosen four benchmark models as presented in Table III to investigate various signature channels. For each of these models, we will compute the event rates for eight supersymmetric discovery channels defined by the following sets of cuts [24,25]

$$\begin{aligned}
&\mathrm{CUT\ C}_1: n(\ell) = 0,\ p_T(j_1) \geq 150\ \mathrm{GeV},\ p_T(j_2, j_3, j_4) \geq 40\ \mathrm{GeV}\\
&\mathrm{CUT\ C}_2: n(\ell) = 0,\ n(b-\mathrm{jets}) \geq 1\\
&\mathrm{CUT\ C}_3: n(j) \geq 4,\ p_T(j_1) \geq 100\ \mathrm{GeV},\ p_T(j_2, j_3, j_4) \geq 40\ \mathrm{GeV},\ \not{E}_T \geq 0.2 m_{\mathrm{eff}}\\
&\mathrm{CUT\ C}_4: n(j) \geq 4,\ p_T(j_1) \geq 100\ \mathrm{GeV},\ m_{\mathrm{eff}} \geq 500\ \mathrm{GeV}\\
&\mathrm{CUT\ C}_5: n(j) + n(\ell) \geq 4,\ p_T(j_1) \geq 100\ \mathrm{GeV},\ H_T^{(4)} + \not{E}_T \geq 500\ \mathrm{GeV}\\
&\mathrm{CUT\ C}_6: n(\ell) = 3,\ n(j) \geq 2,\ p_T(j_2) \geq 40\ \mathrm{GeV}\\
&\mathrm{CUT\ C}_7: n(\ell) = 1,\ p_T(j_1, j_2, j_3, j_4) \geq 40\ \mathrm{GeV},\ \not{E}_T \geq 0.2 m_{\mathrm{eff}}\\
&\mathrm{CUT\ C}_8: \mathrm{Z-veto},\ n(\ell_a^+) = 1,\ n(\ell_b^-) = 1,\ p_T(\ell_2) \geq 20\ \mathrm{GeV}.
\end{aligned} \tag{19}$$

All eight channels involve a cut on transverse sphericity of $S_T \geq 0.2$ and a missing transverse energy cut of $\not{E}_T \geq 100$ GeV, except for CUT C_1 for which we impose $\not{E}_T \geq 150$ GeV. Leptons of the first two generations (e, μ) are denoted collectively by ℓ and the number of leptons and the number of jets in an event are denoted by $n(\ell)$ and $n(j)$ respectively. Similarly, $p_T(\ell_i)$ and $p_T(j_i)$ refer to the transverse momentum of the ith hardest lepton or jet, respectively. The notation $p_T(j_1, j_2, j_3, j_4)$ means that the first through the fourth hardest jets in an event each have to individually pass the cut, and does not imply a sum. If no value is specified for an object, then no cut has been made for that object. In the specification of the cut C_8, the subscripts a and b indicate that the two opposite sign leptons may be of different flavors; a Z-veto is imposed on the invariant mass of the two leptons only in the case when they are of the same flavor, so as to avoid contamination from the Z boson peak produced through standard model production modes.

We define the effective mass $m_{\rm eff}$ and $H_T^{(4)}$ by

$$m_{\rm eff} = \sum_{i=1}^{4} p_T(j_i) + \not{E}_T, \qquad H_T^{(4)} = \sum_{i=1}^{4} p_T(x_i), \qquad (20)$$

where x_i is a visible object (jet or lepton) and the summation, in both cases, is done over the first four hardest objects. The variable $H_T^{(4)}$ is closely related to other definitions of H_T (see [50] for different definitions of H_T). We define a model to be discoverable in a given channel (or for a given cut), C_i, if $N^c_{\rm SUSY} \geq \max\{5\sqrt{N^c_{\rm SM}}, 10\}$, where $N^c_{\rm SUSY}$ is the number of SUSY events and $N^c_{\rm SM}$ is the number of background events. Further, we loosely refer to a 5σ excess as one which satisfies $N^c_{\rm SUSY} \geq 5\sqrt{N^c_{\rm SM}}$, and a lower bound of 10 events is imposed in rare cases where the SM background is insignificant for a specific channel.

In Table IV, we give an analysis of a broad range of event rates for the low mass gaugino models in the Higgs-pole region at $\sqrt{s} = 7$ TeV with both 35 pb^{-1} and 1 fb^{-1} of luminosity under the cuts C_i as defined in Eq. (19). None of the models reach the discovery limit for the case of 35 pb^{-1}. Benchmark point 2 has the largest significance for two reasons: It has the lightest gluino mass of the benchmarks and the second generation squarks are just above the TeV scale. Indeed, these models will produce discoverable signals with an increase of about a factor of 5 in luminosity, which may be expected within the next six to eight months of data-taking. However, any type of serious mass reconstruction will require about an inverse femtobarn of data.

We find that the models analyzed produce a significant amount of jet events. These events arise from gluino decays via off-shell squarks into fermion pairs with a chargino or neutralino, that is, $\tilde{g} \to q_i \bar{q}'_i \tilde{\chi}^{\pm}_1$ and $\tilde{g} \to q_i \bar{q}_i \tilde{\chi}^0_2$ with secondary 3-body decays $\tilde{\chi}^0_2 \to \not{E}_T + 2$ fermions and $\tilde{\chi}^{\pm}_1 \to \not{E}_T + 2$ fermions. Additionally, one has a significant cross section for the direct production of charginos and neutralinos which can also give leptonic final states. Our analysis finds that the distribution of the transverse momentum of the hardest lepton is peaked near $p_T(\ell_1) = 20$ GeV and falls off quickly near 60 GeV before imposing the cuts in Eq. (19). The relatively soft leptonic decay products makes it more difficult to use leptonic signatures as discovery channels with limited data, as exhibited in Table IV. However, the lepton + jets signal can be strong (see channel C_5) where a large significance is achieved. Trileptonic signal C_6 is only at the level of $\sim 2\sigma$ but would become visible with an increase in luminosity by a factor of 6. The above features are generic to all models in the in the sample, given the rigid properties of the gaugino sector shown in Table I.

The strongest signal of new physics will be in the multijet channel. In Fig. 2, we plot the distribution in $m_{\rm eff}$ for two of our benchmark points using the cut C_1 of Eq. (19). The heavy solid line gives the supersymmetric signal events plus the SM background, while the shaded area is the SM background. The peaks in this distribution can be identified with a typical accuracy of 25 GeV, which is half the bin size. A more statistically rigorous approach gives similar results.

Several previous works [51] have shown that there is a relationship between the effective mass peak and the minimum mass of the gluino and the first two generation squark masses. Since in the low mass gaugino models that lie in the Higgs-pole region, the first and the second generation squark masses are always heavier than the gluino mass, the peak of the effective mass gives a relationship to the gluino mass. Further, the only available decay of the gluino is through off-shell squarks. Analyzing the effective mass peak for cut C_1 for all 700 simulated models, we find in general

$$m_{\rm eff}^{\rm peak} \simeq 1.5 m_{\tilde{g}} \quad \text{CUT} \quad C_1, \qquad (21)$$

with the precise range being $m_{\rm eff}^{\rm peak}/m_{\tilde{g}} = 1.57 \pm 0.085$, as can be seen from the distribution in the left panel of Fig. 3. We note that both of the benchmark cases in Fig. 2 show this result explicitly. Thus, a measurement of $m_{\rm eff}^{\rm peak}$ provides an important early clue to the size of the gluino mass. In our discussion below on the $m_{\rm eff}^{\rm peak}$ peak it should

TABLE IV. $N^c_{\rm SUSY}/\sqrt{N^c_{\rm SM}}$ for the models of Table III for both (35 pb^{-1}) and [1 fb^{-1}] of integrated luminosity at the LHC with $\sqrt{s} = 7$ TeV. The (0) in the table means a significance of less than 1. We expect the entire set of our models discussed in Table I to surpass the 5σ significance threshold in jet-based channels early at LHC-7 with about an inverse femtobarn of data.

	Jets $N^c_{\rm SUSY}/\sqrt{N^c_{\rm SM}}$				Leptons+Jets $N^c_{\rm SUSY}/\sqrt{N^c_{\rm SM}}$			
Label	CUT C_1	CUT C_2	CUT C_3	CUT C_4	CUT C_5	CUT C_6	CUT C_7	CUT C_8
1	(2) [12]	(1) [6]	(2) [9]	(2) [11]	(2) [11]	(0) [1]	(1) [3]	(0) [2]
2	(4) [21]	(3) [14]	(4) [21]	(4) [24]	(4) [23]	(0) [2]	(1) [6]	(0) [1]
3	(3) [13]	(1) [10]	(2) [13]	(3) [15]	(3) [15]	(0) [2]	(1) [5]	(0) [2]
4	(2) [15]	(2) [10]	(2) [13]	(3) [16]	(3) [15]	(1) [2]	(1) [5]	(0) [2]

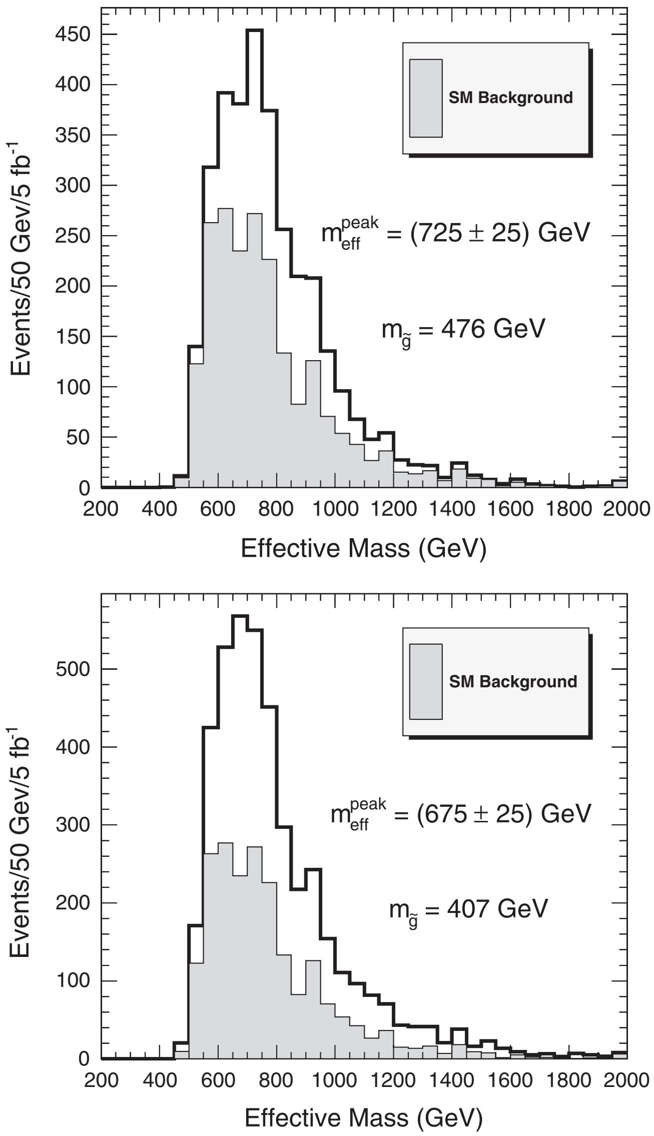

FIG. 2. (color online) Effective mass variable $m_{\rm eff}$ for the SUSY signal plus background with cut C_1 at $\sqrt{s} = 7$ TeV. The SM background alone is shown shaded for comparison. For benchmark 1 (top panel), with a gluino mass of 476 GeV, we see a peak at $m_{\rm eff} = (725 \pm 25)$ GeV corresponding to a mass ratio of $m_{\rm eff}^{\rm peak}/m_{\tilde g} = 1.52 \pm 0.055$. For benchmark 2 (bottom panel), with a gluino mass of 407 GeV, a peak is observed at $m_{\rm eff} = (675 \pm 25)$ GeV which corresponds to a mass ratio of $m_{\rm eff}^{\rm peak}/m_{\tilde g} = 1.66 \pm 0.065$.

be kept in mind that the results are valid for our specific cut within the model class. Next, defining

$$\Delta m \equiv m_{\tilde\chi_2^0} - m_{\tilde\chi_1^0} = (\alpha_{\tilde\chi_2^0} - 1) m_{\tilde\chi_1^0}, \tag{22}$$

the mass relations found in Eq. (13) or Eq. (14) suggest that under cut C_1 the peak in the effective mass distribution will be proportional to Δm

$$\frac{m_{\rm eff}^{\rm peak}}{\Delta m} \simeq 1.5 \times \frac{m_{\tilde g}}{(\alpha_{\tilde\chi_2^0} - 1) m_{\tilde\chi_1^0}} = 1.5 \times \frac{\alpha_{\tilde g}}{(\alpha_{\tilde\chi_2^0} - 1)}. \tag{23}$$

The distribution of $m_{\rm eff}^{\rm peak}/\Delta m$ is shown to be peaked in the right panel of Fig. 3, a result which follows from the left panel of Fig. 3 and from the distribution in $\alpha_{\tilde g}$ shown previously in Fig. 1.

The mass ratio plotted in the right panel in Fig. 3 is noteworthy in that the quantity Δm is measurable from the edge of the opposite-sign, same-flavor (OSSF) dilepton invariant mass distribution, $m_{\ell^+\ell^-}^{\rm edge}$ (for a recent study, see [52]). In Fig. 4, we plot this distribution for the same two benchmark models from Fig. 2 after applying the cuts C_5 from Eq. (19).

Upon reconstruction of the dilepton invariant mass for the two sample models, one observes clean edges near 55 GeV and 60 GeV for the two cases. For the complete set of the 700 simulated models, one finds

$$\begin{aligned} m_{\ell^+\ell^-}^{\rm edge} &\le m_{\tilde\chi_2^0} - m_{\tilde\chi_1^0} = (\alpha_{\tilde\chi_2^0} - 1) m_{\tilde\chi_1^0} \\ &= \begin{cases} 0.75 m_{\tilde\chi_1^0} & \text{minimum} \\ 1.07 m_{\tilde\chi_1^0} & \text{maximum.} \end{cases} \end{aligned} \tag{24}$$

In addition, from Eq. (13) we expect the upper bound of the OSSF dilepton plot to be less then 65 GeV which is the upper limit on Δm found in the analysis which can be understood by using the appropriate predictions for the α_i for each model point. We remark that formally the $m_{\ell^+\ell^-}$ relation above is an inequality arising from the angular dependence of the kinematic inner product, however given enough luminosity it becomes close to an equality.

In addition, because $m_{\ell^+\ell^-}^{\rm edge} \le \Delta m$, we can express the effective mass peak in terms of the edge approximately as

$$m_{\ell^+\ell^-}^{\rm edge} \lesssim \frac{2}{3} \times \frac{\alpha_{\tilde\chi_2^0} - 1}{\alpha_{\tilde g}} m_{\rm eff}^{\rm peak}. \tag{25}$$

Thus we arrive at a very simple, but strong, correlation between these two key observables at the LHC, i.e., $m_{\ell^+\ell^-}^{\rm edge}$ and $m_{\rm eff}^{\rm peak}$.

We therefore come to the conclusion that the low mass gaugino models in the Higgs-pole region are fully testable with early LHC data. If the models studied in this paper do indeed describe the supersymmetric content of our Universe, then the following three observations must follow:

(1) The dilepton invariant mass edge with an upper bound of $(\alpha_{\tilde\chi_2^0} - 1) m_{\tilde\chi_1^0} \le 65$ GeV must be found. If a dilepton invariant mass edge is not observed in this range with several fb^{-1} of integrated luminosity, this model would be falsified.
(2) The multijet effective mass must be found, which peaks in the range 550 GeV $\lesssim m_{\rm eff}^{\rm peak} \lesssim$ 800 GeV consistent with Eq. (21).
(3) The mass relation in Eq. (25) must hold.

We now emphasize

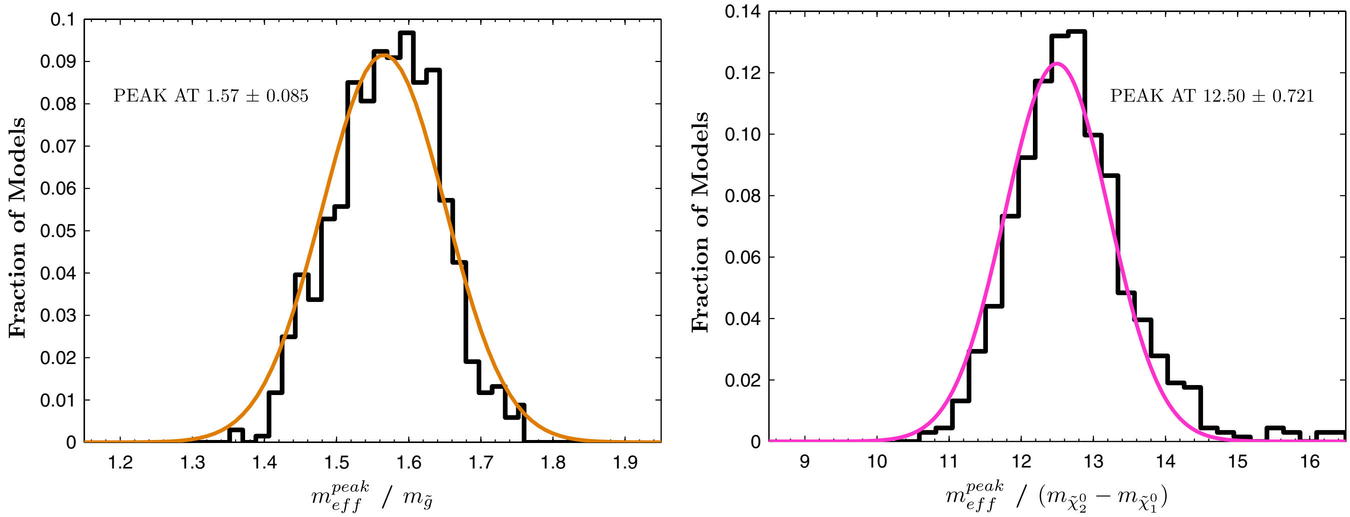

FIG. 3 (color online). Left: Distribution of the ratio of the effective mass peak to the gluino mass. The models plotted here are the 700 model subset and the peak is found after adding the SM background and applying cut C_1. We find the peak to be at 1.57 ± 0.085. Right: Distribution of the ratio of effective mass peak to the mass difference between the two lightest neutralinos under the same cut. The mass difference between the two lightest neutralinos corresponds to the upper bound of the edge in the OSSF dilepton invariant mass plot. We find the peak to be at 12.50 ± 0.721.

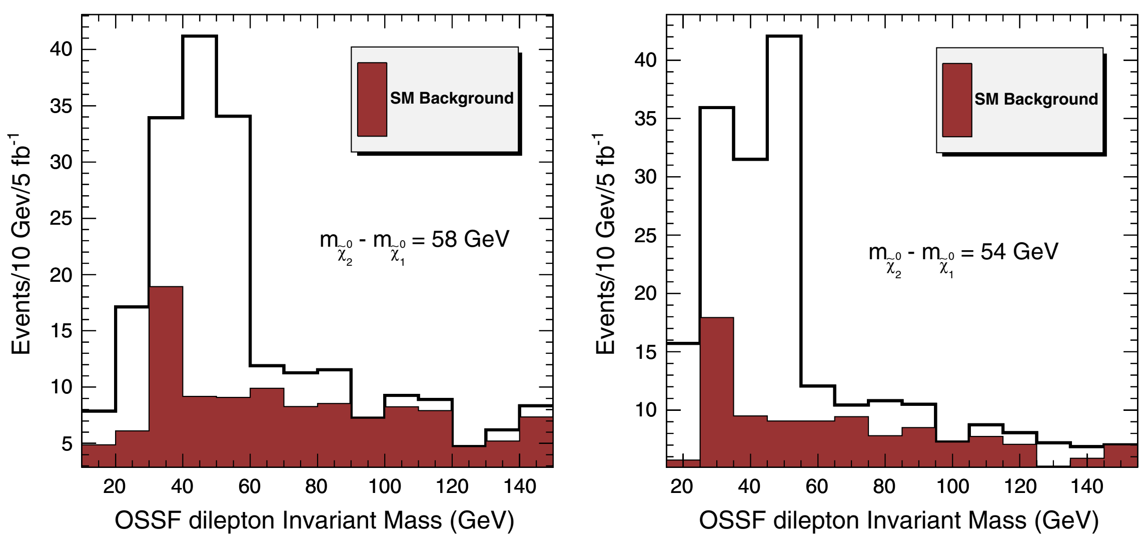

FIG. 4 (color online). OSSF dilepton invariant mass for the SUSY signal plus SM background using cut C_5 at $\sqrt{s} = 7$ TeV. The SM background is shown separately for comparisons. For the benchmark 1 (left panel) we see an edge at $m_{\ell^+\ell^-}^{\text{edge}} = 60 \pm 5$ GeV and for the benchmark 2 (right panel) we see an edge at $m_{\ell^+\ell^-}^{\text{edge}} = 55 \pm 5$ GeV, which agree well with the mass differences between the two lightest neutralinos in both cases, which are predicted to be 60 GeV and 55 GeV from theory (see Table III).

(i) LHC measurements can be used to estimate the dark matter mass in this model class. The upper bound of the edge in the OSSF dilepton invariant mass allows us to estimate the neutralino mass splitting and the scaling relation of Eq. (24) allows us to infer the dark matter mass.

(ii) The effective mass peak and the dilepton invariant mass edge are strongly correlated via Eq. (25) and provide cross-checks of the model.

While the analysis here focuses on universal boundary conditions at the unification scale, one may ask how the situation could change with nonuniversal boundary conditions, particularly in the gaugino masses. Indeed, a lower dilepton mass edge could be possible with nonuniversal gaugino masses allowing for a compatible relic density through the Z-pole instead of the Higgs-pole. If the mass splitting between the second heaviest neutralino and LSP is of appropriate size the position of the edge could potentially support an overlap with the Higgs-pole models. However, here the LSP mass would be close to $M_Z/2$ and opposed to $m_h/2$. With this ambiguity in the position of the edge, since the LSP dark matter masses would differ by (10–20) GeV or so between the Higgs-pole and Z-pole models, the models could be distinguished not only via dark matter direct detection experiments (to be discussed) but also via their other LHC signals. This is why it becomes necessary to examine multiple signatures at the LHC. The ultimate cross check of the Higgs-pole models corresponds to the LHC observing the light Higgs boson in the ~(110–130) GeV mass range, and dark matter direct detection experiments observing events in mass range ~(50–65) GeV.

In the next section, we will look for further avenues to exploit the remarkable predictivity of the Higgs-pole model paradigm.

IV. DARK MATTER DIRECT DETECTION EXPERIMENTS AND CONNECTION TO THE LHC

The complementarity between dark matter detection experiments and collider signatures has been emphasized in many previous works (for a recent review, see [3]). Here, we will focus on this complementarity within the context of the low mass gaugino models in the Higgs-pole region. We will show that experiments for the direct detection of dark matter such as XENON put further constraints on the parameter space of the model.

We begin by noting that the predictions of Eqs. (10) and (12), and the relic density constraint largely ensure that the models yield predictions in narrow corridors as exhibited in Table I. Nevertheless, the properties of the neutralino, and, in particular, its scattering cross section on nucleons, will depend on parameters such as μ, $\tan\beta$ and the resultant components n_{1j} which govern the wave function of the LSP. The features of the spin-independent neutralino-nucleon scattering are easily understood in the models as they arise for large m_0 with the s-channel squark exchange suppressed and the scattering is dominated by Higgs exchange through the t-channel. Thus, the spin-independent scattering off target nucleus T arising via the interaction $C_i\tilde{\chi}_1^0\tilde{\chi}_1^0\bar{q}_iq_i$, in the limit of small momentum transfer is well approximated by $\sigma^{\rm SI}_{\tilde{\chi}_1^0 T} = (4\mu^2_{\tilde{\chi}_1^0 T}/\pi)(Zf_p + (A-Z)f_n)^2$ with $f_{p/n} = \sum_{q=u,d,s} f^{(p/n)}_{T_q} C_q \frac{m_{p/n}}{m_q} + \frac{2}{27} f^{(p/n)}_{TG} \sum_{q=c,b,t} C_q \frac{m_{p/n}}{m_q}$ with the form factors $f^{(p/n)}_{T_q}$, $f^{(p/n)}_{TG}$ given in [32,53–55] and with coupling given by [53–55]

$$C_q = -\frac{g_2 m_q}{4m_W B}\Big[\Re(\delta_1[g_2 n_{12} - g_Y n_{11}]) DC\Big(-\frac{1}{m_H^2} + \frac{1}{m_h^2}\Big) + \Re(\delta_2[g_2 n_{12} - g_Y n_{11}])\Big(\frac{D^2}{m_h^2} + \frac{C^2}{m_H^2}\Big)\Big]. \quad (26)$$

The parameters $\delta_{1,2}$ depend on eigen components of the LSP wave function and B, C, D depend on VEVs of the Higgs fields and the neutral Higgs mixing parameter α. For up quarks one has $(\delta_1, \delta_2, B, C, D) = (n_{13}, n_{14}, s_\beta, s_\alpha, c_\alpha)$ and for down quarks $(\delta_1, \delta_2, B, C, D) = (n_{14}, -n_{13}, c_\beta, c_\alpha, -s_\alpha)$. These simple relations reproduce numerical results of [32] and closely match the numerical work we do in this paper.

For the four benchmark models of Table III, we present the spin-independent cross section of neutralino scattering on protons in Table V. However, from a survey over the collection of all the models in the Higgs-pole region, we find a very broad range of possible scattering cross sections

$$4\times 10^{-47}\ {\rm cm}^2 \lesssim \sigma^{\rm SI}_{\tilde{\chi}_1^0 p} \lesssim 4\times 10^{-42}\ {\rm cm}^2. \quad (27)$$

The largest of these are already ruled out experimentally from the null results of the CDMS-II and XENON 100 experiments [30,31]. For the purposes of this paper, we will assume a hard limit of $\sigma^{\rm SI}_{\tilde{\chi}_1^0 p} \leq 6\times 10^{-44}$ cm^2 for all neutralino masses under consideration as indicated by the XENON 100 experiment; this value is extremely conservative as their reported bounds are a factor of 2 more stringent, but we wish to allow for some uncertainty. A large fraction of the remaining models will be probed after longer exposures with XENON, or in future at other experiments. The distribution of our 12 000 models in the $(m_{\tilde{\chi}_1^0}, \sigma^{\rm SI}_{\tilde{\chi}_1^0 p})$ plane is given in Fig. 5 with both the CDMS-II and XENON 100 limits indicated [30,31]. Models which are being constrained by the XENON and CDMS data are those with $50 < \tan\beta < 60$. Note that the models in Fig. 5 satisfy all the constraints discussed in Sec (II).

An important point to note is that dark matter direct detection experiments can be used to learn about soft supersymmetry breaking parameters. Figure 5 shows that once the spin-independent cross section and neutralino mass are known from direct detection experiments, then $m_{1/2}$ can be determined directly. Let us assume that a dark matter direct detection experiment observes a signal in the near future which is compatible with a neutralino LSP in the mass range 50 GeV $\lesssim m_{\tilde{\chi}_1^0} \lesssim$ 65 GeV. Within the constraints of the of the Higgs-pole region, even a crude measurement of the scattering cross section yields important information about the parameters of the model. The

TABLE V. Spin-independent cross section for neutralino scattering on protons for the benchmark models of Table III. Also given is the computed thermal relic density and the components n_{1j} of the LSP wave function.

Label	$\sigma^{\rm SI}_{\tilde{\chi}_1^0 p}$cm^2	$n_{11}(\tilde{B})$	$n_{12}(\tilde{W})$	$n_{13}(\tilde{H}_1)$	$n_{14}(\tilde{H}_2)$	$\Omega_{\rm CDM}h^2$
1	1.4×10^{-46}	0.995	−0.023	0.093	−0.015	0.110
2	1.7×10^{-46}	0.998	−0.029	0.058	−0.012	0.108
3	1.8×10^{-44}	0.996	−0.018	0.092	−0.012	0.104
4	3.0×10^{-44}	0.996	−0.016	0.085	−0.011	0.125

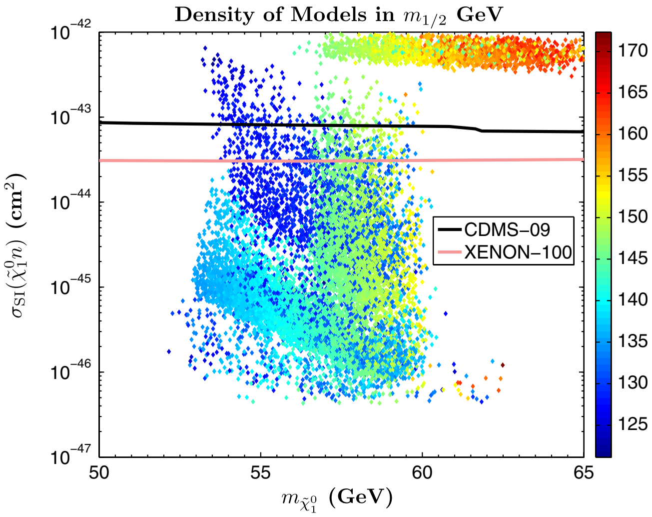

FIG. 5 (color online). The spin-independent cross section $\sigma^{SI}_{\tilde{\chi}_1^0 p}$ versus neutralino mass. Points are colored according to the value of $m_{1/2}$ taken. Applying the XENON and CDMS limits, we see that $m_{1/2}$ is preferred in the 120 GeV to 155 GeV region.

results shown in Fig. 5 already demonstrate a correlation between $\sigma^{SI}_{\tilde{\chi}_1^0 p}$ and $m_{1/2}$. For example, a simultaneous estimation of $m_{\tilde{\chi}_1^0} \sim 55$ GeV and $\sigma^{SI}_{\tilde{\chi}_1^0 p} \sim 2 \times 10^{-45}$ cm^2 would predict 125 GeV $\lesssim m_{1/2} \lesssim 140$ GeV due to the correlated nature of the parameters within the Higgs-pole region. This, in turn, would have testable consequences for the gaugino sector at the LHC.

The XENON bound can be mapped into a constraint on m_A. This constraint is more restrictive than the one from collider bounds. Without direct detection constraints, a pseudoscalar mass as low as $m_A \simeq 190$ GeV is allowed, as it satisfies the Tevatron search limits as well as the indirect constraints imposed above. For example, one such model in Fig. 5 has $m_A = 190$ GeV, $\tan\beta = 56$, $m_{\tilde{\chi}_1^0} = 60$ GeV, $n_{11} = 0.994$ and $n_{13} = 0.102$; for this particular model, $\sigma^{SI}_{\tilde{\chi}_1^0 p} \sim 5.5 \times 10^{-43}$ cm^2 in excess of what is allowed by XENON 100 data. Thus the XENON constraint is stronger than the Tevatron bound for this point. More generally, we obtain a limit arising from the dark matter direct detection constraint:

$$m_A \gtrsim 300 \text{ GeV} \qquad \text{XENON Constraint.} \tag{28}$$

Including uncertainties in the form factors that enter the computation of $\sigma^{SI}_{\tilde{\chi}_1^0 p}$, one may loosen or tighten this constraint a bit; however, the point here is that the constraints on m_A become rather strong from the XENON data. The value quoted above is particular to the requirements within the confines of the scaling predictions in Eq. (10) and the mass range Eq. (12). However, other models with radiative electroweak symmetry breaking are also strongly constrained. We have performed a separate analysis to investigate minimal supergravity models which satisfy the WMAP constraints of Eq. (11) via stau-co-annihilation, which have a heavier neutralino mass than the models studied here (owing to mass limits on the stau) and we find that the present XENON data imposes only a slightly weaker lower bound of $m_A \gtrsim 250$ GeV. Constraints of this type have been studied in SUGRA models [56] and in generic weak scale MSSM models in Refs. [57,58] and more recently in the context of low mass dark matter in Refs. [59–61]. The results presented here show that for dark matter in the 50 GeV region, the constraints on the CP-odd Higgs sector in models of radiative breaking are also quite strong. We anticipate that the lower bound on m_A will only get stronger as additional data from XENON arrives (for projections, see e.g. [62]).

It is interesting to note that Eq. (28) is precisely the mass scale for which the LHC will be sensitive to the production of the pseudoscalar Higgs with 1 fb^{-1} at $\sqrt{s} = 7$ TeV [63]. It is therefore possible to probe the pseudoscalar Higgs at LHC-7 in the $2\tau + b$-tagged jets channel within a subset of the models. In conjunction with the measurements of Eq. (26) this could serve to extract the value of $\tan\beta$. We therefore exhibit the subset of the 12 000 models with large $\tan\beta$ in Fig. 6 and plot $\tan\beta$ vs the CP-odd

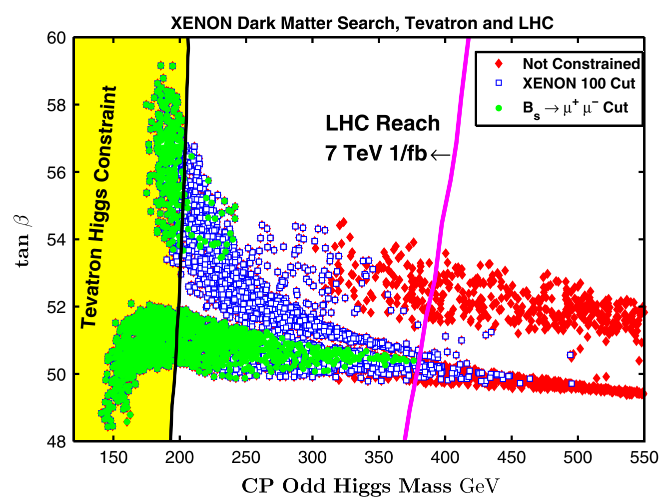

FIG. 6 (color online). Displayed is the small subset of the 12 000 models which are those corresponding to large $\tan\beta$ and with low m_A within reach of LHC-7 in the first year (a majority of the 12 000 models have heavier m_A and lie off this graph). The LHC estimated projected reach (magenta curve) with isolated tau pairs and b-tagging [63] is indicated. Models ruled out by the XENON 100 experiment [30] are in blue (squares) and we have taken a conservative cut $\sigma^{SI}_{\tilde{\chi}_1^0 p} \leq 6 \times 10^{-8}$ pb to account for theoretical and experimental uncertainties. Red (diamonds) are allowed models in this mass range of $(m_A, \tan\beta)$. Constraints on sparticle mass limits as well as other constraints are imposed as discussed in Sec. II; however the models ruled out by the $B_s \to \mu^+\mu^-$ constraint are shown explicitly in green (circles) to illustrate its effects. The shaded yellow region indicates where the Tevatron has excluded m_A. We conclude that the XENON 100 constraints are very severe in this part of the parameter space.

Higgs m_A. The heavy black line (yellow shaded region) is the Tevatron direct search limit, while green points are eliminated from Tevatron constraints on $\mathrm{Br}(B_s \to \mu^+\mu^-)$. Blue squares represent models that are eliminated by the (conservative) imposition of $\sigma^{\mathrm{SI}}_{\tilde{\chi}^0_1 p} \leq 6 \times 10^{-44}\ \mathrm{cm}^2$ from XENON 100 results. The red points are the surviving models with $m_A \leq 550$ GeV and the estimated LHC-7 reach for 1 fb^{-1} is shown by the (solid) nearly vertical magenta curve. We note that there are a number of cases which could give detectable signals at the LHC, and in addition, a substantial portion these models correspond to spectrum with a light *CP*-odd Higgs mass which have a neutralino mass and spin-independent cross section that lie close to the range of observation relevant to the XENON experiment.

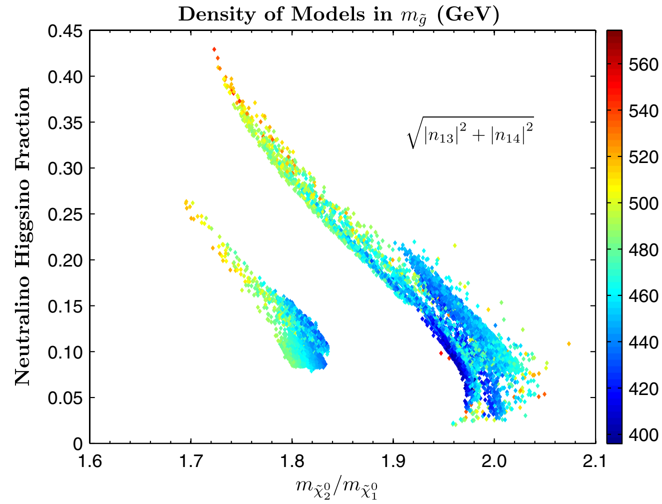

FIG. 7 (color online). Higgsino eigencontent of the LSP displayed as a function of $\alpha_{\tilde{\chi}^0_2} = m_{\tilde{\chi}^0_2}/m_{\tilde{\chi}^0_1}$. The models are indicated by the gluino mass. Once $\alpha_{\tilde{\chi}^0_2}$ is measured via corroborating evidence at the LHC and in dark matter detection, and the gluino mass is deduced at the LHC, the Higgsino eigencontent, $\sqrt{|n_{13}|^2 + |n_{14}|^2}$ may be determined.

V. DETERMINING GAUGINO AND HIGGSINO CONTENT OF THE LSP AND THE SOFT PARAMETERS FROM THE INTERSECTION OF DARK MATTER AND LHC DATA

In this section, we will further connect the LHC to dark matter detection. In particular, the data from both types of experiments can be combined to extract information on the soft SUSY breaking parameters as well as the eigencontent of the neutralino LSP.

A. Determining Eigencontent of the Neutralino LSP

Let us assume that dark matter direct detection experiments have determined (or at least restricted) the possible range of LSP mass and spin-independent cross section. Unfortunately, in the models, this information leaves the LSP eigencontent in terms of gaugino and Higgsino components still undetermined. The model points in Fig. 5 in the $(m_{\tilde{\chi}^0_1}, \sigma^{\mathrm{SI}}_{\tilde{\chi}^0_1 p})$ plane that are unconstrained by the XENON data have large fluctuations in their Higgsino content. Hence, we need to turn to LHC data in concert with direct detection data in order to sort this out. The two types of measurements at the LHC required are the ones discussed above: a measurement of the edge in the OSSF dilepton invariant mass and a measurement of $m^{\mathrm{peak}}_{\mathrm{eff}}$. Taken together with dark matter detection results, these quantities can help determine the eigencontent of the LSP as we now show.

Previously, we have seen that a measurement of the edge in the OSSF dilepton invariant mass at the LHC gives us an upper bound on Δm, the mass difference between the two lightest neutralinos (see Eq. (24)). Taken together with the LSP mass measured by dark matter experiments as well as the LHC, this information then gives an experimental determination of the mass ratio $m_{\tilde{\chi}^0_2}/m_{\tilde{\chi}^0_1} = 1 + \Delta m/m_{\tilde{\chi}^0_1}$. This quantity is the horizontal axis in Fig. 7.

Additionally, a measurement of $m^{\mathrm{peak}}_{\mathrm{eff}}$ at the LHC gives us a good estimate of $m_{\tilde{g}}$, as can be seen in Eqs. (21) and (16). In Fig. 7 we have shaded the model points according to the value of $m_{\tilde{g}}$. Hence, given this information together with the value of $m_{\tilde{\chi}^0_2}/m_{\tilde{\chi}^0_1}$ along the horizontal axis allows us to estimate the Higgsino fraction of the LSP plotted along the vertical axis. Thus, one can then essentially read off the Higgsino eigencontent of the neutralino dark matter from Fig. 7. Clearly this determination will be rough due to uncertainties at every stage, but it provides a first step in the determination of the gaugino vs Higgsino eigencontent of the LSP.

In complementary fashion, once dark matter experiments can measure the lightest neutralino mass one can then determine $\alpha_{\tilde{g}}$ as well (see Eq. (23)). Finally, we note that in the limiting case when the models approach the pure bino limit for the neutralino, it is seen from Fig. 7 that the ratio of the second lightest neutralino to the LSP approaches 2 and the gluino mass is driven towards its lowest value. In summary, these observables combined together would lend strong support for the model class.

B. Determination of A_0/m_0

The density of possible values of the ratio of soft SUSY breaking parameters A_0/m_0 in the models from our scan is shown in Fig. 8, on a plot of $\sigma^{\mathrm{SI}}_{\tilde{\chi}^0_1 p}$ versus $m_{\tilde{\chi}^0_2}/m_{\tilde{\chi}^0_1}$. Let us now assume that dark matter experiments have determined $\sigma^{\mathrm{SI}}_{\tilde{\chi}^0_1 p}$ as well as $m_{\tilde{\chi}^0_1}$. One can see that current bounds on $\sigma^{\mathrm{SI}}_{\tilde{\chi}^0_1 p}$ as discussed in the previous section already rule out some ranges of A_0/m_0. Most of the remaining models congregate around $A_0/m_0 \sim \pm 1$.

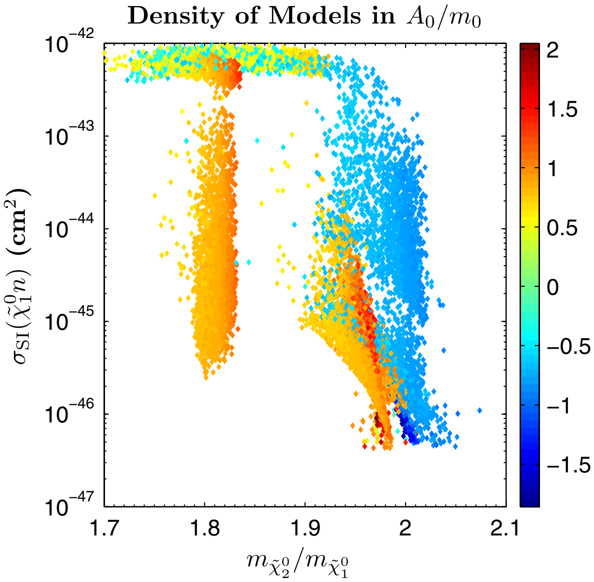

FIG. 8 (color online). $\sigma^{\rm SI}_{\tilde{\chi}_1^0 p}$ versus $m_{\tilde{\chi}_2^0}/m_{\tilde{\chi}_1^0}$ distributed in A_0/m_0. The ratio A_0/m_0 exists in separate regions relative to $m_{\tilde{\chi}_2^0}/m_{\tilde{\chi}_1^0}$ and knowledge of the OSSF edge at the LHC can point to the soft parameter space.

As in the previous subsection, the horizontal axis $m_{\tilde{\chi}_2^0}/m_{\tilde{\chi}_1^0}$ can be determined by a combination of LSP mass obtained from dark matter experiments (as well as LHC) together with Δm determined from a measurement of the edge in the OSSF dilepton invariant mass at the LHC. As future bounds on $\sigma^{\rm SI}_{\tilde{\chi}_1^0 p}$ improve, some further information on A_0/m_0 will be attained.

It is interesting that the combination of the two types of experiments could help determine the scalar trilinear A_0 relative to m_0 as the trilinear couplings are otherwise difficult to measure from the LHC data alone. As an explicit example to the above general statements, models with $A_0/m_0 \simeq 1$ are found to have a mass splitting between $\tilde{\chi}_2^0$ and $\tilde{\chi}_1^0$ of 45 GeV $\leq \Delta m \leq$ 50 GeV. The models with Δm near the upper limit of the allowed range favors the opposite case with $A_0/m_0 \simeq -1$. In addition, the majority of the models which congregate around $\alpha_{\tilde{\chi}_2^0} = m_{\tilde{\chi}_2^0}/m_{\tilde{\chi}_1^0} <$ 1.8 are ruled out by XENON. Indeed, as emphasized in the previous section, the LHC should be able to determine the dark matter mass of any of the models with the largest uncertainty at about the 20% level.

VI. CONCLUSION

We have analyzed a predictive model relevant to early SUSY discovery at the LHC at $\sqrt{s} = 7$ TeV. We claim that within the framework of minimal supergravity unification, models with ~50 GeV dark matter must be found in early LHC data, or they will be ruled out. Our analysis was targeted at the mass scale where the LSP can have a mass of this size consistent with astrophysical and particle physics constraints, and where the relic density of dark matter is largely governed by the presence of the light *CP* even Higgs-pole. Connected are the mass of the relic lightest neutralino, and the gluino mass, the latter of which has an upper bound of about 575 GeV in this model class. Such a gluino can be detected in the early runs at the LHC from its distinctive decay signatures consisting of energetic leptons and jets along with a sizeable missing energy.

The model can be further checked in direct detection experiments such as XENON via a detection of event rates consistent with the spin-independent neutralino-proton cross section $\sigma^{\rm SI}_{\tilde{\chi}_1^0 p}$ which has a theoretical upper bound near 10^{-42} cm^2 while a large collection of these models tend to be in the range $\sigma^{\rm SI}_{\tilde{\chi}_1^0 p} = 10^{-46\pm1}$ cm^2. In connection with the above, we showed that the current experimental limits from XENON 100 already put limits on the model and lead to a lower bound on the *CP*-odd Higgs mass of $m_A \gtrsim 300$ GeV, which is more stringent than the current constraints from direct searches for the production of the pseudoscalar from the Tevatron.

It was further shown that measurements of certain signatures at the LHC can allow one to estimate the neutralino mass and the gluino mass with the LHC data. With sufficient luminosity, the kinematic edge in the OSSF dilepton invariant mass distribution directly allows one to estimate the neutralino dark matter mass due to scaling in the gaugino sector; namely, the ratio of the masses of two lightest neutralinos are related by a scale factor, and this scale factor is close to 2. Similarly, from the $m_{\rm eff}$ distribution, one can infer the gluino mass.

If the low mass gaugino models within the Higgs-pole region studied in this paper do indeed describe the supersymmetric content of our Universe, then there are three absolute predictions which must be found in the data. First, the location of the dilepton invariant mass should be seen in a narrow range near 50 GeV. Since this mass edge is very close to the mass of the dark matter particle, its measurement will determine the dark matter mass to ~20%. Second, the multijet effective mass under our cuts will peak in the range 550 GeV $\lesssim m_{\rm eff}^{\rm peak} \lesssim$ 800 GeV. Since this peak is related to the gluino mass via $m_{\rm eff}^{\rm peak} \sim 1.5 \times m_{\tilde{g}}$, this measurement will give a first estimate in the determination of the mass of the gluino. Third, we have deduced a simple relation between the peak in the effective mass and the dilepton invariant mass edge via Eq. (25) that can be checked directly with LHC data.

In addition, it was shown that the intersection of constraints from the LHC and direct detection experiments provide further information about the SUSY model. A combination of accelerator and direct detection data sets can provide estimates of $\tan\beta$ and A_0/m_0; can tell us about the gaugino and Higgsino content of the dark matter; and can provide information about the mass of the dark matter particle. The model class is consistent with the very recent

ATLAS and CMS data with 35 pb^{-1}. A most exciting feature of the analysis given here is that the required data to test the model will be taken in the very near future.

ACKNOWLEDGMENTS

This research is supported in part by Department of Energy (DOE) Grant No. DE-FG02-95ER40899 and by the Michigan Center for Theoretical Physics, and the U.S. National Science Foundation (NSF) Grant Nos.PHY-0653342, PHY-0704067 and PHY-0757959, and in addition by the NSF through TeraGrid resources provided by National Center for Supercomputing Applications (NCSA), Texas Advanced Computing Center (TACC), Purdue University and Louisiana Optical Network Initiative (LONI) under Grant No. TG-PHY100036. KF thanks the Texas Cosmology Center (TCC). TCC is supported by the College of Natural Sciences and the Department of Astronomy at the University of Texas at Austin and the McDonald Observatory. KF also thanks the Aspen Center for Physics for hospitality during her visit.

[1] A. H. Chamseddine, R. L. Arnowitt, and P. Nath, Phys. Rev. Lett. **49**, 970 (1982); L. J. Hall, J. D. Lykken, and S. Weinberg, Phys. Rev. D **27**, 2359 (1983).
[2] R. Arnowitt and P. Nath, Phys. Rev. Lett. **69**, 725 (1992).
[3] P. Nath, B. D. Nelson, D. Feldman *et al.*, Nucl. Phys. B, Proc. Suppl. **200-202**, 185 (2010).
[4] G. Kane *et al.*"*Perspectives on Supersymmetry* (World Scientific, Singapore, 2010) p. 583, Vol. 2.
[5] P. Nath, arXiv:hep-ph/0307123.
[6] L. E. Ibanez and G. G. Ross, C.R. Physique **8**, 1013 (2007).
[7] E. Komatsu *et al.* (WMAP Collaboration), Astrophys. J. Suppl. Ser. **192**, 18 (2011); Astrophys. J. Suppl. Ser. **170**, 377 (2007); **148**, 119 (2003).
[8] P. Nath and R. L. Arnowitt, Phys. Rev. Lett. **70**, 3696 (1993); J. L. Lopez, D. V. Nanopoulos, and K. j. Yuan, Phys. Rev. D **48**, 2766 (1993); M. Drees and A. Yamada, Phys. Rev. D **53**, 1586 (1996); H. Baer and M. Brhlik, Phys. Rev. D **53**, 597 (1996); V. D. Barger and C. Kao, Phys. Rev. D **57**, 3131 (1998); T. Nihei, L. Roszkowski, and R. Ruiz de Austri, J. High Energy Phys. 05 (2001) 063.
[9] A. Djouadi, M. Drees, and J. L. Kneur, Phys. Lett. B **624**, 60 (2005).
[10] K. Nakamura *et al.* (Particle Data Group Collaboration), J. Phys. G **37**, 075021 (2010).
[11] For a review see: M. S. Carena and H. E. Haber, Prog. Part. Nucl. Phys. **50**, 63 (2003); H. E. Haber, J. Phys. Conf. Ser. **259**, 012017 (2010).
[12] R. Barate *et al.*, Phys. Lett. B **565**, 61 (2003).
[13] CDF and D0 Collaboration, arXiv:1007.4587.
[14] D. Feldman, Z. Liu, and P. Nath, Phys. Rev. Lett. **99**, 251802 (2007).
[15] D. Feldman, Z. Liu, and P. Nath, J. High Energy Phys. 04 (2008) 054.
[16] D. Feldman, Z. Liu, and P. Nath, Phys. Rev. D **81**, 095009 (2010).
[17] U. Chattopadhyay, D. Das, D. K. Ghosh, and M. Maity, Phys. Rev. D **82**, 075013 (2010).
[18] B. Altunkaynak, B. D. Nelson, L. L. Everett, Y. Rao, and I. W. Kim, arXiv:1011.1439.
[19] S. Cassel, D. M. Ghilencea, S. Kraml, A. Lessa, and G. G. Ross, J. High Energy Phys. 05 (2011) 120.
[20] S. P. Martin and M. T. Vaughn, Phys. Lett. B **318**, 331 (1993).
[21] D. M. Pierce, J. A. Bagger, K. T. Matchev, and R. j. Zhang, Nucl. Phys. **B491**, 3 (1997).
[22] D. Feldman, G. Kane, R. Lu, and B. D. Nelson, Phys. Lett. B **687**, 363 (2010); E. Izaguirre, M. Manhart, and J. G. Wacker, J. High Energy Phys. 12 (2010) 030; G. F. Giudice, T. Han, K. Wang, and L. T. Wang, Phys. Rev. D **81**, 115011 (2010); N. Bhattacharyya, A. Datta, and S. Poddar, Phys. Rev. D **82**, 035003 (2010); B. C. Allanach, S. Grab, and H. E. Haber, J. High Energy Phys. 01 (2011) 138; M. A. Ajaib, T. Li, Q. Shafi, and K. Wang, J. High Energy Phys. 01 (2011) 028; G. Kane, E. Kuflik, R. Lu, and L. T. Wang, arXiv:1101.1963; P. Bandyopadhyay and B. Bhattacherjee, arXiv:1012.5289; S. Bhattacharya and S. Nandi, arXiv:1101.3301.
[23] H. Baer, V. Barger, A. Lessa, and X. Tata, J. High Energy Phys. 06 (2010) 102.
[24] B. Altunkaynak, M. Holmes, P. Nath, B. D. Nelson, G. Peim, Phys. Rev. D **82**, 115001 (2010).
[25] N. Chen, D. Feldman, Z. Liu, P. Nath, and G. Peim, Phys. Rev. D **83**, 035005 (2011); N. Chen *et al.*, Phys. Rev. D **83**, 023506 (2011).
[26] V. Khachatryan *et al.* (CMS Collaboration), Phys. Lett. B **698**, 196 (2011).
[27] (ATLAS Collaboration) Report No. CERN-PH-EP-2011-013, [Phys. Rev. Lett. (to be published)]; http://cdsweb.cern.ch/record/1328281.
[28] P. Nath and R. L. Arnowitt, Mod. Phys. Lett. A **2**, 331 (1987); R. L. Arnowitt, R. M. Barnett, P. Nath, and F. Paige, Int. J. Mod. Phys. A **2**, 1113 (1987); H. Baer and X. Tata, Phys. Rev. D **47**, 2739 (1993); V. D. Barger, C. Kao, and T. j. Li, Phys. Lett. B **433**, 328 (1998); E. Accomando, R. L. Arnowitt, and B. Dutta, Phys. Lett. B **475**, 176 (2000); Z. Sullivan and E. L. Berger, Phys. Rev. D **78**, 034030 (2008).
[29] H. Baer, C. h. Chen, F. Paige, and X. Tata, Phys. Rev. D **52**, 2746 (1995); **50**, 4508 (1994).
[30] E. Aprile *et al.* (XENON100), Phys. Rev. Lett. **105**, 131302 (2010).

[31] Z. Ahmed *et al.*(CDMS-II), Phys. Rev. Lett. **102**, 011301 (2009);
[32] G. Belanger, F. Boudjema, A. Pukhov., A. Semenov, Comput. Phys. Commun. **180**, 747 (2009).
[33] P. Nath and R. L. Arnowitt, Phys. Lett. B **289**, 368 (1992).
[34] A. Djouadi, J. L. Kneur, and G. Moultaka, Comput. Phys. Commun. **176**, 426 (2007).
[35] M. Muhlleitner, A. Djouadi, and Y. Mambrini, Comput. Phys. Commun. **168**, 46 (2005); A. Djouadi, M. M. Muhlleitner, and M. Spira, Acta Phys. Pol. B **38**, 635 (2007).
[36] A. Djouadi, M. Drees, and J. L. Kneur, J. High Energy Phys. 03 (2006) 033.
[37] N. Chen, D. Feldman, Z. Liu, and P. Nath, Phys. Lett. B **685**, 174 (2010).
[38] T. Aaltonen *et al.* (CDF Collaboration), Phys. Rev. Lett. **100**, 101802 (2008).
[39] E. Barberio *et al.* (Heavy Flavor Averaging Group), arXiv:0808.1297.
[40] M. Misiak *et al.*, Phys. Rev. Lett. **98**, 022002 (2007).
[41] K. L. Chan, U. Chattopadhyay, and P. Nath, Phys. Rev. D **58**, 096004 (1998); R. L. Arnowitt and P. Nath, Phys. Rev. D **46**, 3981 (1992); J. L. Feng, K. T. Matchev, and T. Moroi, Phys. Rev. Lett. **84**, 2322 (2000); U. Chattopadhyay, A. Corsetti, and P. Nath, Phys. Rev. D **68**, 035005 (2003); H. Baer, C. Balazs, A. Belyaev, T. Krupovnickas, and X. Tata, J. High Energy Phys. 06 (2003) 054; D. Feldman, Z. Liu, and P. Nath, Phys. Rev. D **78**, 083523 (2008).
[42] (CDF Collaboration), Phys. Rev. Lett. **101**, 251801 (2008).
[43] (D0 Collaboration), Phys. Lett. B **680**, 34 (2009).
[44] J. Strologas (CDF Collaboration), AIP Conf. Proc. **1200**, 275 (2010).
[45] W. Beenakker, R. Hopker, M. Spira, and P. M. Zerwas, Nucl. Phys. **B492**, 51 (1997); W. Beenakker, M. Klasen, M. Kramer, T. Plehn, M. Spira, and P. M. Zerwas, Phys. Rev. Lett. **83**, 3780 (1999).
[46] J. Alwall, P. Demin, S. de Visscher, R. Frederix, M. Herquet, F. Maltoni, T. Plehn, D. Rainwater, and T. Stelzer, J. High Energy Phys. 09 (2007) 028.
[47] T. Sjostrand, S. Mrenna, and P. Z. Skands, J. High Energy Phys. 05 (2006) 026.
[48] PGS-4, J. Conway *et al.*, conway/research/software/pgs/pgs4-general.htm
[49] J. A. Maxin, V. E. Mayes, and D. V. Nanopoulos, Phys. Rev. D **79**, 066010 (2009); C. F. Berger, J. S. Gainer, J. L. Hewett, and T. G. Rizzo, J. High Energy Phys. 02 (2009) 023; P. Konar, K. T. Matchev, M. Park, and G. K. Sarangi, Phys. Rev. Lett. **105**, 221801 (2010).
[50] A. Barr, C. Lester, J. Phys. G **37**, 123001 (2010).
[51] I. Hinchliffe, F. E. Paige, M. D. Shapiro *et al.*, Phys. Rev. D **55**, 5520 (1997); D. R. Tovey, Phys. Lett. B **498**, 1 (2001); R. Kitano and Y. Nomura, Phys. Rev. D **73**, 095004 (2006).
[52] N. Mohr, arXiv:0904.3408.
[53] U. Chattopadhyay, T. Ibrahim, and P. Nath, Phys. Rev. D **60**, 063505 (1999).
[54] P. Gondolo and K. Freese, J. High Energy Phys. 07 (2002) 052;
[55] J. R. Ellis, A. Ferstl, and K. A. Olive, Phys. Lett. B **481**, 304 (2000).
[56] D. Feldman, Z. Liu, and P. Nath, Phys. Lett. B **662**, 190 (2008).
[57] M. S. Carena, D. Hooper, and A. Vallinotto, Phys. Rev. D **75**, 055010 (2007).
[58] J. Hisano, K. Nakayama, and M. Yamanaka, Phys. Lett. B **684**, 246 (2010).
[59] D. Feldman, Z. Liu, and P. Nath, Phys. Rev. D **81**, 117701 (2010).
[60] E. Kuflik, A. Pierce, and K. M. Zurek, Phys. Rev. D **81**, 111701 (2010).
[61] D. Vasquez, G. Belanger, C. Boehm, A. Pukhov, J. Silk, Phys. Rev. D **82**, 115027 (2010).
[62] E. Aprile, L. Baudis (XENON), Proc. Sci., DM2008 (2008) 018.
[63] CMS Collaboration, Report No. CMS NOTE 2010/008; See also: D.L. Pegna, MCTP & UMATLAS Conference on LHC First Data, 2010; M. Sani, arXiv:1012.0159; D. Benjamin *et al.* (Tevatron New Phenomena & Higgs Working Group), arXiv:1003.3363.